공학석사학위논문

바나듐 레독스 흐름 전지 응용을 위한 폴리벤지미다졸/그래피틱 카본나이트라이드 나노시트 복합막 개발

Polybenzimidazole/Graphitic Carbon Nitride Nanosheets Composite Membranes for Vanadium Redox Flow Battery Applications

2020년 2월

서울대학교 대학원

화학생물공학부

조 경 화

Abstract

Polybenzimidazole/Graphitic Carbon Nitride Nanosheets Composite Membranes for Vanadium Redox Flow Battery Applications

Kyunghwa Cho

Polymer Chemistry

Department of Chemical & Biological Engineering

Seoul National University

Polybenzimidazole(PBI) has been widely used as an ion exchange membrane for vanadium redox flow batteries (VRFBs) because of its ultralow vanadium ions permeability and high chemical stability. However, its relatively low proton conductivity causes poor single cell performance compared to commercial Nafion

membranes. Herein, PBI composite membranes were prepared with different weight ratios of graphitic carbon nitride nanosheets (g-C_3N_4) which were obtained by thermal oxidation and exfoliation process. The structural properties of g-C_3N_4 nanosheets provide additional acid doping sites and promote to form stable proton transport channels. The sulfuric acid doping level and water uptake of PBI/g-C_3N_4 composite membranes were measured and PBI/g-C_3N_4_1.0 had the highest value. As a result, the proton conductivity of PBI/g-C_3N_4_1.0 was higher than PBI pristine and other composite membranes. PBI and PBI/g-C_3N_4_1.0 membranes showed extremely low vanadium ion permeability in comparison to the Nafion membrane. In the VRFB single cell performance test, the energy efficiency of the PBI/g-C_3N_4_1.0 composite membrane exhibited higher than that of the pristine PBI membrane. The PBI/g-C_3N_4 composite membranes maintained the outstanding chemical stability of PBI in the *ex-situ* oxidative stability test.

Keywords: Polybenzimidazole, Graphitic carbon nitride, Composite membrane, Ion exchange membrane, Vanadium redox flow battery

Student Number: 2018-22675

List of Tables

List of Scheme

List of Figures

List of Contents

1. Introduction

As one of the solutions to the rapidly growing energy demand around the world, the need for an energy storage system (ESS) is increasing to enable efficient energy supply. ESS stores energies from the surplus electricity produced during the night time and intermittent renewable energy and ensures electricity to be delivered when it is needed.[1, 2] Currently, the second batteries mainly used as an energy storage device in ESS are lithium-ion batteries. However, there are disadvantages such as short lifespan, a limitation for large capacity and high risk of fire and explosion.[3] To date, vanadium redox flow batteries (VRFB) have been considered as one of the most promising candidates for addressing these issues because of its attractive features such as durability, long lifespan, large-scale energy storage ability, and safety.[4] The VRFB system comprises four different oxidation states of vanadium ions as two redox couples in sulfuric acid, V^{2+}/V^{3+} in anolyte and VO^{2+}/VO_2^{+} in catholyte, stored in separate electrolyte reservoirs. The vanadium redox couple reactions do not produce any toxic gases, and thus there is low risk of explosion. In

addition, since all active species are the same element unlike other flow batteries, VRFBs could be away from permanent damage caused by cross-contamination.[5, 6]

Ion exchange membrane (IEM), which is the key component of VRFBs, serves not only as a separator of positive and negative electrolytes but also as a medium for proton conduction. The requirements for ideal IEMs are, therefore, high proton conductivity, low vanadium ion permeability, high chemical stability in acidic conditions, as well as low price.[7]

At present, the Dupont's Nafion, which is a perfluorosulfonic acid membrane, has been widely utilized in VRFBs with its excellent chemical stability and superior proton conductivity.[8] However, Nafion membranes suffer from serious problems. For example, severe vanadium ion crossover arisen from its large ion transport channel could make the poor cell performance. Also, exorbitant cost accounting for around 40% of the total price of the cell stack renders the full commercialization of VRFBs difficult.[9] Consequently, considerable efforts have been directed towards the development of high-performance hydrocarbon membranes that are cost-effective and feature high ion selectivity.[7]

Polybenzimidzole (PBI), which is a notably attractive option as an alternative to perfluorosulfonic acid membranes, has high chemical stability and ultralow vanadium permeability compared to sulfonated hydrocarbon membranes.[10] Although PBI itself is an electrically inert polymer possessing very low ion-conducting ability, the proton conductivity of PBI can be endowed by doping with strong acids such as sulfuric acid or phosphoric acid.[11] To enhance the conductivity of PBI, which is still lower than that of Nafion, numerous improvement methods were devised; typical methods are to make cross-linking structure using ionic or covalent bonds[12-14], to graft side chains into the polymer backbone[2, 15], and to prepare composite membranes by adding nano-sized fillers[16, 17].

The graphitic carbon nitride (g-C_3N_4) nanosheets are graphene-like 2D materials, which can be produced from cheap melamine by simple thermal oxidation.[18, 19] The laminar structure and triangular nanopores of g-C_3N_4 nanosheets help to from stable proton conducting channels. [20] Moreover, a lot of NH/NH_2 groups in g-C_3N_4 can offer additional acid doping sites.[19]

In this study, g-C_3N_4 nanosheets were embedded into a PBI matrix to prepare

PBI/g-C_3N_4 nanocomposite membrane for VRFB applications, expecting the increase of low proton conductivity of PBI. The general properties such as acid doping level, water uptake, proton conductivity, vanadium permeability and chemical stability were investigated. Also, single cell performance of PBI and PBI/g-C_3N_4 composite membranes were assessed.

2. Experimental

2.1. Materials

3,3′-Diaminobenzidine (DAB, ≥99%), isophthalic acid (99%), melamine (99%), vanadium(V) oxide (99.99%, trace metals basis), and polyphosphoric acid (PPA, reagent grade, 115% H_3PO_4 basis) were purchased from Aldrich. Vanadium(IV) sulfate oxide hydrate (99.9%, metals basis) was obtained from Alfa Aesar. Sulfuric

acid (95%), sodium hydroxide (NaOH, 97%) and magnesium sulfate (99%) were acquired by Daejung Chemicals. N-methyl-2-pyrrolidone (NMP, 99%) was provided by Junsei chem. Co. and it was stored over molecular sieves. All other reagents and solvents were handled as received. Nafion115 was supplied by Dupont company and its thickness is 127μm.

2.2. Synthesis of polybenzimidazole (PBI)

PBI was synthesized via solution condensation reaction between 3,3′-Diaminobenzidine (DAB) and isophthalic acid. DAB (3g, 14mmol) and isophthalic acid (2.44g, 14mmol) was added and 65mL of PPA was poured into the 250mL three-neck round bottom flask equipped with nitrogen inlet and outlet, and mechanical stirrer. The mixture was maintained at 150℃ for 15h to dissolve the reactants. Subsequently, the solution was heated to 250℃ and lasted for 2.5h. The resultant solution was precipitated in deionized water. The collected polymer was

washed with deionized water several times and treated with sodium hydroxide to remove the excess PPA. Again, the polymer was washed several times with deionized water to be neutralized. Lastly, the final product was filtered and dried in vacuum oven for 2 days at 60°C.

2.3. Preparation of graphitic carbon nitride nanosheets (g-C_3N_4)

Bulk(b-C_3N_4) and graphitic carbon nitride(g-C_3N_4) were prepared as previously reported.[18, 19] First, b-C_3N_4 was prepared by thermal oxidation of melamine (3g) in a furnace at the temperature of 550°C for 3h with a heating rate of 3°C/min. For the "etching" process, the obtained yellow powder was heated again with a rate of 3°C/min until it reached at 500°C and lasted for 2 h. The final product, g-C_3N_4, had a light yellow color.

2.4. Preparation of PBI and PBI/g-C_3N_4 composite membranes

All membranes including PBI and PBI/g-C_3N_4 composite membranes were prepared by a solution casting method. For both PBI and composite membranes, 2.0 wt% of PBI powder was dissolved in NMP at 80℃ with stirring. In case of the nanocomposite membranes, the g-C_3N_4 nanosheets filler was dispersed in the PBI/NMP solution with different mass percent to PBI; the mixture was stirred at 70℃ for 24h and sonicated for 1h. The prepared solution was carefully cast onto a clean flat glass and the amount of the solution was adjusted to control the thickness of a membrane. After drying at 80℃ for 15 h and at 120℃ for 5 h, membranes were peeled off from the glass in deionized water and dried on a vacuum plate. For acid-doping, all membranes were immersed in the 4M H_2SO_4 solution at room temperature for 48 h before use. The prepared composite membranes were denoted as PBI/g-C_3N_4_X, where X is the weight percentage of g-C_3N_4 nanosheets to PBI.

2.5. Characterization of PBI, g-C_3N_4 and composite membranes

The ^{1}H-NMR spectra was collected on Avance-400 (Bruker, Germany) with a proton frequency of 400 MHz. Deuterated dimethylsulfoxide (DMSO-d6) and tetramethylsilane (TMS) were used as the solvent and the internal standard, respectively. Fourier-transform infrared (FT-IR) spectra of samples were recorded on Nicolet 6700 (Thermo Scientific, USA) in the attenuated total reflectance (ATR) mode in the frequency range of 4000 to 650 cm^{-1}. The spectra were collected over 30 scans at 4 cm^{-1} resolutions. X-ray diffraction (XRD) patterns were acquired with RI-GAKU MODE 1 SMARTLAB using a monochromatic CuKα (1.5406 Å) radiation. X-ray photoelectron spectroscopy (XPS) was recorded on a Sigma probe (Thermo Scientific) using Al Kα (1254.0 eV) as the radiation source. Data were collected in a range of 0–1300 eV, followed by a high-resolution scan of the C 1s and N 1s regions. The morphologies of the membranes were inspected by JSM-6701F (JEOL, Japan) using a field emission scanning electron microscope (FE-

SEM). For the inspection of cross-sectional morphology, samples were prepared by cutting the liquid nitrogen-quenched membranes. Transmisson Electron Microscope (TEM) images were taken by using JEM-3010 (JEOL Ltd, Japan) under an operating voltage of 200 keV. The samples for TEM were prepared by drop casting DIW/Acetone dispersion on Quantifoil holey carbon TEM grid and dried in oven at 60℃.

2.5.1. Acid doping level, water uptake and dimensional change

The membranes were cut into $1\text{cm} \times 3\text{cm}$ and were dried in a vacuum oven at 80℃ for 2 days. The volumes (V_0) and weights (W_0) of the samples were measured. Then, the membranes were immersed in 4M H_2SO_4 solutions at room temperature for 2 days. The membranes were wiped with Kimwipes to remove the excess acid solution on the membrane surface, and their volumes (V_1) and weights (W_1) were measured again. Finally, the hydrated and acid-doped membranes were dried at 80℃

under vacuum for 2 days to measure the weights (W_2) of membrane after evaporating the water completely. The acid doping level (ADL), Water uptake (WU) and volume change (ΔV) were calculated by the following equations.

$$\text{ADL} = \frac{(W_2 - W_0)/M_{H_2SO_4}}{W_0/M_{PBI}} \quad (1)$$

$$\text{WU} = \frac{W_1 - W_2}{W_0} \times 100 \quad (2)$$

$$\Delta\text{V}(\%) = \frac{V_1 - V_0}{V_0} \times 100 \quad (3)$$

where $\text{M}_{\text{H}_2\text{SO}_4}$ and M_{PBI} are the molecular weights of sulfuric acid and the repeat unit of the PBI, respectively.

2.5.2. Proton conductivity

The proton conductivity of membranes was obtained from the area resistance

values, which were measured using an impedance analyzer with two-probe clip-cell. The measurement was carried out in the bath filled with 4M H_2SO_4 solutions and the area resistance (AR) was calculated from the following equation.

$$\mathrm{AR} = (\mathrm{R}_1 - R_2) \times S \tag{4}$$

where R_1 and R_2 are the electrical resistance of the cell with and without a membrane and S ($0.196 cm^2$) is the effective area.

The proton conductivity of each membrane was calculated using the area resistance value by the following equation.

$$\sigma = \mathrm{L}/(\mathrm{A} \times \mathrm{R}) \tag{5}$$

where L is the thickness of the membrane, A is the effective area and R is the resistance of the membrane.

2.5.3. Vanadium permeability and selectivity

The vanadium permeability was determined by measuring the diffusion rate of VO^{2+} across the membrane. The membrane was sandwiched by two half-cells, where the left cell was filled with 1.5M $VOSO_4$ in 3M H_2SO_4 solution (80mL) and the right cell was filled with 1.5M $MgSO_4$ in 3M H_2SO_4 solution (80mL) to prevent the effect of osmotic pressure. The both side of solutions were continuously stirred to minimize concentration polarization. The 3mL of sample solution of right cell was taken every 24h and the VO^{2+} concentration of the sample was detected by UV-vis spectrometer (U-5100, HITACHI) at the wavelength of 765 nm.[1] The solution was put back into the right cell after the measurement. The vanadium permeability (P) was calculated according to Fick's diffusion law as shown in the following equation.

$$\mathrm{V_R}\ \frac{d(C_R(t))}{dt} = \mathrm{A}\frac{P}{L}\left(\mathrm{C_L} - C_R(t)\right) \qquad (6)$$

where V_R is the volume of solution in the right cell, t is time, $C_R(t)$ is the concentration of VO^{2+} in the right cell as a function of time and CL is the initial concentration of VO^{2+} in the left cell. P is the VO^{2+} permeability, A is the effective

area of membrane (3.14 cm^2) and L is the thickness of the membrane.

2.5.4. VRFB single cell test

The VRFB single cell was equipped by two carbon felt electrodes separated by the membrane with an effective area of 7×7 cm^2 and two graphite bipolar plates and two copper plates serving as a current collector were clamped together. The VRFB single cell was operated by a battery cycler (Scribner Associates Inc., 857 redox cell test system) under various current densities from 40$mAcm^{-1}$ to 100$mAcm^{-1}$ at room temperature. The 100mL of 1.63M $V^{3.5+}$ in 4.29M H_2SO_4 solution was used for both positive and negative electrolytes, with the flow rate of 100$mLmin^{-1}$. The cut off voltages of charging and discharging were set as 1.6-1.0V to avoid the corrosion of electrodes and bipolar plates. The coulombic efficiency (CE), voltage efficiency (VE) and energy efficiency (EE) of the cell were calculated by following equations.

$$\text{CE (\%)} = \frac{\int I_d dt}{\int I_c dt} \times 100 \quad (7)$$

$$\text{EE (\%)} = \frac{\int V_d I_d dt}{\int V_c I_c dt} \times 100 \quad (8)$$

$$\text{VE (\%)} = \frac{EE}{CE} \times 100 \quad (9)$$

where V, I and t are the voltage, current and time, respectively and the subscripts c and d correspond to the charge and discharge processes, respectively.

2.6. *Ex* situ chemical stability

The chemical stability of membranes was assessed by the *ex situ* immersion method using a highly oxidizing VO^{2+} solution as reported previously.[2, 21] Before the test, the membranes were rinsed in isopropyl alcohol for 2 days to remove any impurities and dried in a vacuum oven at 80℃ for 24h. Afterward, each

membrane(18mg) was immersed and kept in the 20mL of 0.1 M VO_2^+/3M H_2SO_4 solution at 40℃. The VO^{2+} concentration change of each solution was monitored over time using the UV-vis spectrometer in the wavelength of 760nm.

3. Result and Discussion

3.1. Preparation of PBI and g-C_3N_4 nanosheets

PBI was polymerized by condensation reaction between DAB and isophthalic acid using PPA as a solvent (Scheme 1).[22] The chemical structure of PBI was confirmed by ^{1}H-NMR spectroscopy (Fig. 1). Synthesized PBI had an inherent viscosity of 1.9 dL g^{-1} in H_2SO_4 solution at 25°C.

As illustrated in Scheme 2, g-C_3N_4 was prepared by thermal oxidation and exfoliation. The structure of g-C_3N_4 was investigated by FT-IR and XPS. In FT-IR spectrum of g-C_3N_4 (Fig. 2a), there is a broad band near 3200cm^{-1} which is assigned to terminal NH or NH_2 groups and the peak at 883cm^{-1} is attributed to the deformation mode of NH groups. Besides, the peaks near 3500cm^{-1} in the spectrum of melamine disappeared in g-C_3N_4. The presence of tri-s-triazine is confirmed by two parts. The one is a sharp peak at 805cm^{-1}, which is attributed to the out-of-plane

bending vibration of tri-s-triazine ring structure.[19] The other is the region comprising strong peaks at 1300-1700cm^{-1}, which is originated from the stretching vibration of the centered N-$(C)_3$ bonds or bridging C-NH-C units.[23] The XPS result also showed the characteristic peaks of g-C_3N_4. In C1s spectra (Fig. 2c), three peaks at binding energies of 288.6 eV, 288.1 eV and 284.9 eV were found through the curve fitting program, which can be attributed to the C-N-C, C-$(N)_3$ and C-C groups, respectively.[24] The deconvolution of the N1s curve (Fig. 2d) also revealed three different peaks at binding energies of 401.1 eV, 399.6 eV and 398.8 eV. The first and third peaks were assigned to the terminal amino groups (C-N-H) and sp^2 nitrogen atoms (C-N=C). The second peak was originated from the bridging tertiary nitrogen atoms (N-$(C)_3$), which cannot be found in the melamine structure.[25] Besides, atomic C/N ratio (0.74) as determined by XPS analysis, was a good agreement with g-C_3N_4 composition.

The crystallinity of g-C_3N_4 nanosheets was investigated by their XRD patterns. (Fig. 3a) Two characteristic diffraction peaks were observed from both bulk and graphitic carbon nitride. The strong peak at the position of 27.7^{o} (d = 0.322nm)

corresponds to the interlayer stacking of aromatic (002) lattice planes. The relatively weak peak located at 12.9^{o} ($d = 0.686nm$) is derived from the (100) in-plane distance between tri-s-triazine units, indicating the presence of triangular nanopores in the synthesized carbon nitrides.[26] In the case of g-C_3N_4, the intensity of both peaks decreased in comparison to b-C_3N_4, which demonstrates that the exfoliation of g-C_3N_4 nanosheets has successfully occurred.[27]

The morphology of g-C_3N_4 was also investigated by TEM. As shown in Fig. 3b, the prepared g-C_3N_4 demonstrates sheet-like morphology. The size of g-C_3N_4 nanosheet observed through TEM image was approximately 340nm.

Scheme 1. Synthesis of polybenzimidazole (PBI)

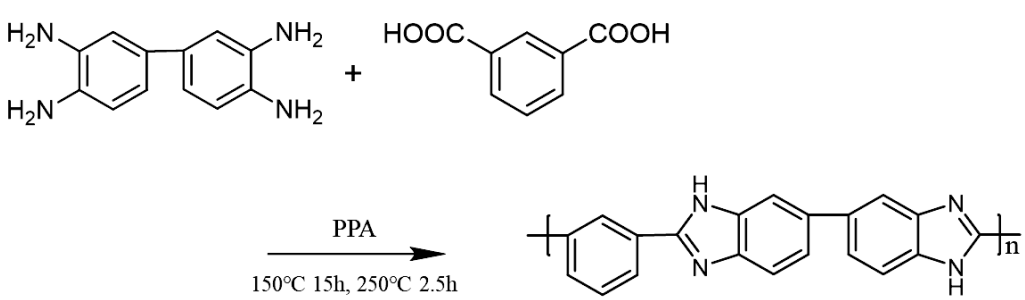

Scheme 2. Preparation of graphitic carbon nitride nanosheets (g-C_3N_4)

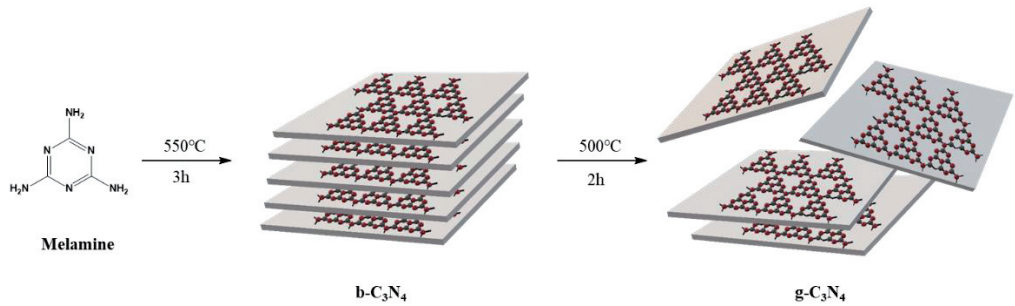

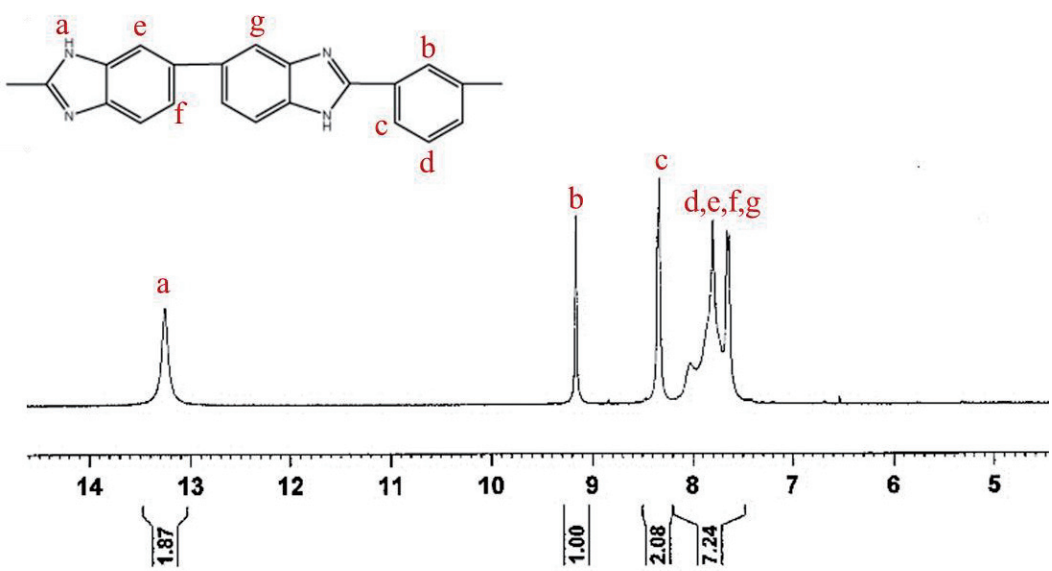

Figure 1. ^{1}H NMR Spectrum of PBI

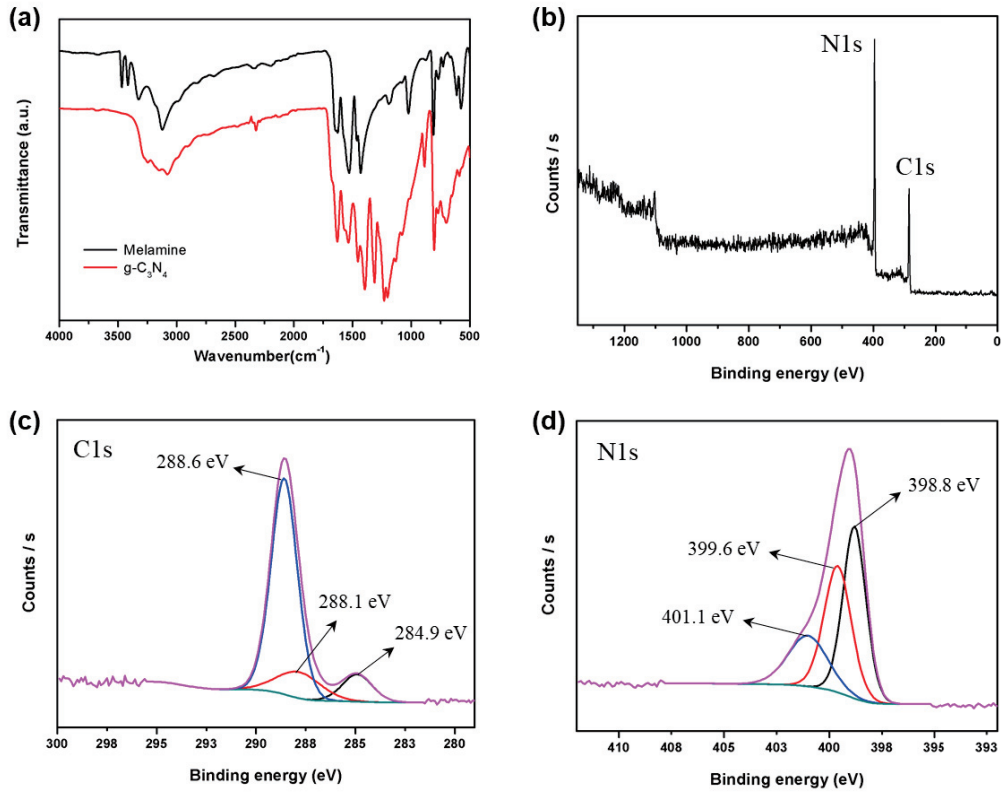

Figure 2. FT-IR spectra of melamine and g-C_3N_4 (a). XPS spectra of g-C_3N_4 (b), C1s (c) and N1s (d).

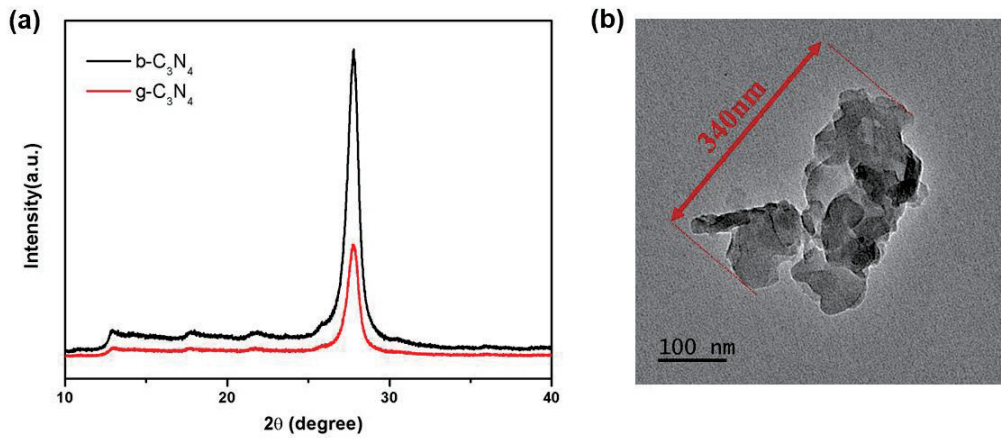

Figure 2. (a) XRD patterns of b-C_3N_4 and g-C_3N_4. (b) TEM image of g-C_3N_4.

3.2. Structure and morphology of composite membranes

The PBI/g-C_3N_4 composite membranes were successfully prepared by a solution casting method with the thickness of 20-40μm. The composite membranes were characterized by FT-IR (Fig. 4). The FT-IR spectrum of the PBI pristine membrane was similar to that of composite membranes because PBI contains imidazole groups which have characteristic peaks similar to triazole groups in g-C_3N_4.[28] Nonetheless, the presence of filler could be confirmed from the new peaks in the region of 1200-1650cm^{-1} which are originated from the bridging bonds (N-$(C)_3$ or C-NH-C) between tri-s-triazine units in the spectrum of composite membranes.[29]

The information of dispersion state of fillers was obtained by SEM analysis. The cross-section images of PBI and PBI/g-C_3N_4 composite membranes were shown in Fig. 5. The typical cross-sectional image of PBI without any cracks was acquired [30, 31] and the overall morphology did not change when the g-C_3N_4 fillers

were introduced into PBI. In the enlarged images, g-C_3N_4 in composite membranes containing less than 1.5 wt% are smaller and have a smooth interface with the polymer matrix, which means nanofillers were well dispersed. However, the large agglomerate of fillers was observed in PBI/g-C_3N_4_1.5 and PBI/g-C_3N_4_2.0 membranes because of the aggregation of g-C_3N_4 nanosheets. It is known that the aggregation of g-C_3N_4 nanosheets easily occurs during the slow solvent evaporation which is inevitable process in the membrane preparation step.[27] Furthermore, the aggregation was effortlessly found in the surface images of PBI/g-C_3N_4_1.5 and PBI/g-C_3N_4_2.0 membranes, which was not detected in that of pristine PBI and PBI/g-C_3N_4_1.0 membranes (Fig. 6). The aggregation of fillers in nanocomposite membranes engender an obstructed the ionic transfer pathway.[19, 32] Therefore, it can be concluded that the optimum content of g-C_3N_4 nanosheets should be lower than 1.5wt%.

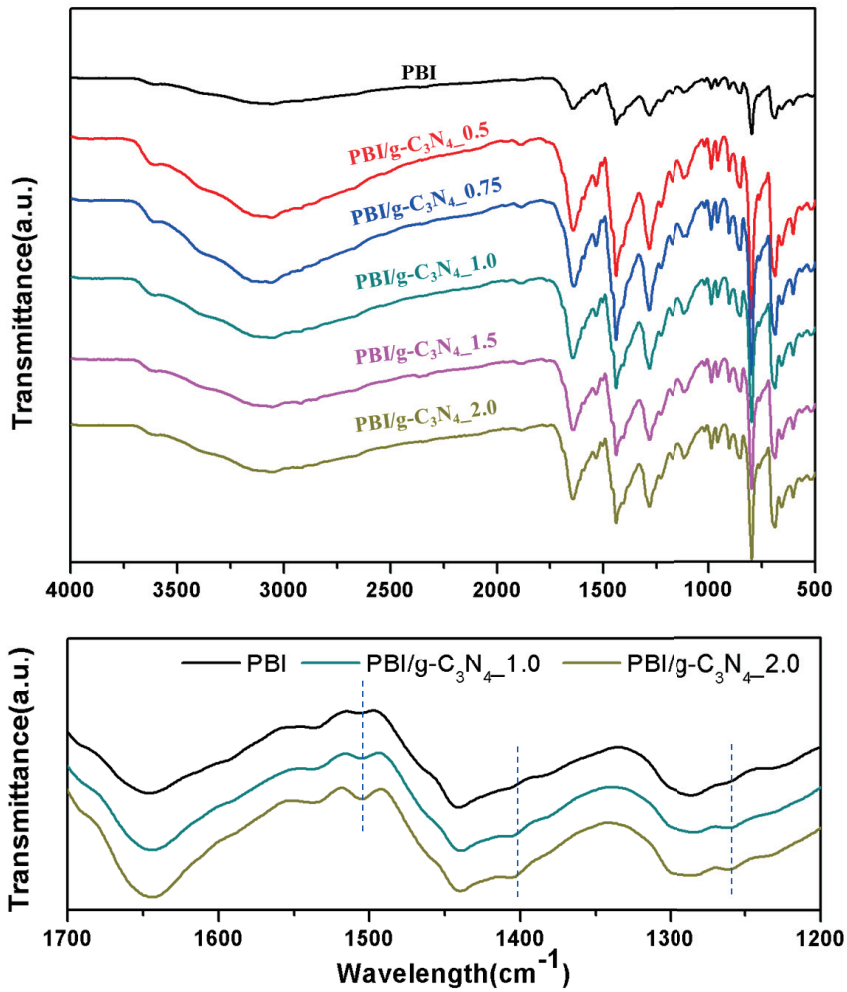

Figure 4. FT-IR spectra of PBI and PBI/g-C_3N_4 composite membranes.

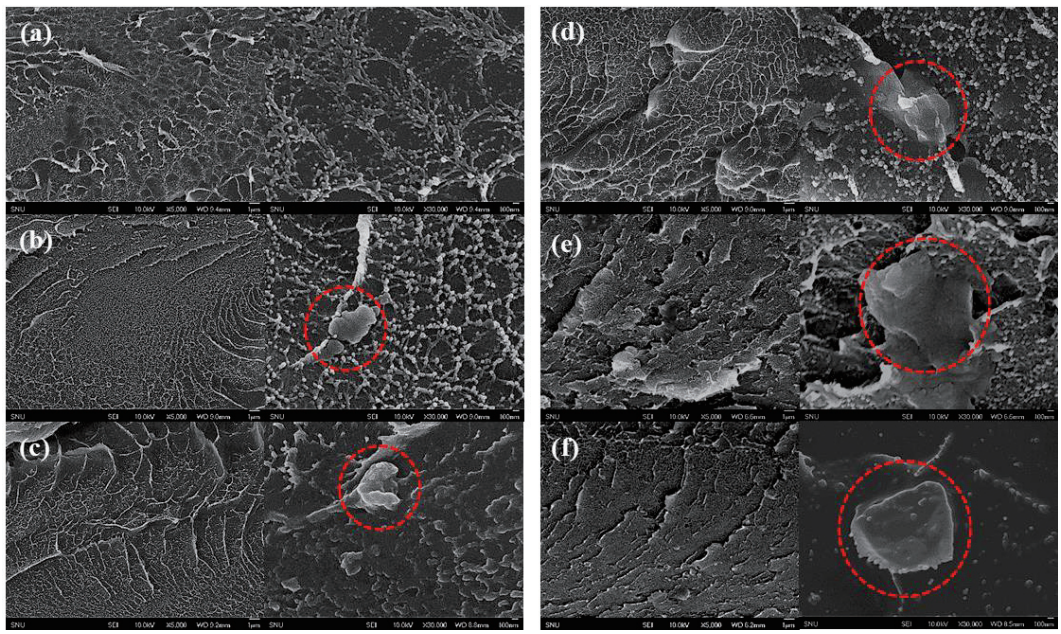

Figure 5. Cross-sectional SEM images of PBI (a) PBI/g-C_3N_4_0.5 (b), PBI/g-C_3N_4_0.75 (c), PBI/g-C_3N_4_1.0 (d), PBI/g-C_3N_4_1.5 (e), PBI/g-C_3N_4_2.0 (f).

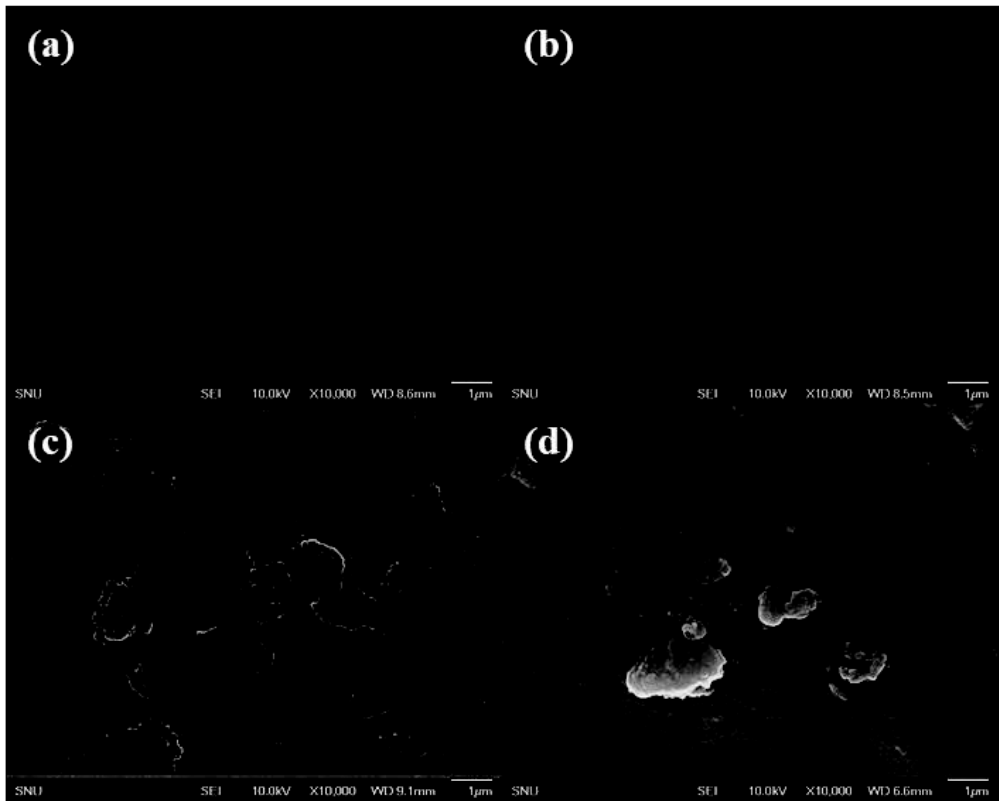

Figure 6. Surface SEM images of PBI (a), PBI/g-C_3N_4_1.0 (b), PBI/g-C_3N_4_1.5 (c), PBI/g-C_3N_4_2.0 (d).

3.3. Acid doping level, water uptake and dimensional change

In general, the proton conductivity of PBI is greatly dictated by the amount of absorbed acid and water because a sufficient number of acid groups and water molecules facilitate the formation of proton transport channels.[33] The physicochemical properties including acid doping level (ADL), water uptake (WU) and dimensional change (ΔV) are shown in Table 1 and Figure 7. The ADL, WU and ΔV of PBI and all composite membranes were investigated after immersed in the 4M H_2SO_4 solution for 48hours at room temperature. The ADL increased until the filler content reaches at 1.0wt% owing to the additional acid doping site from nitrogen atoms in g-C_3N_4. The WU also increased with the incorporation of g-C_3N_4 up to 1.0wt% because the triangular nanopores and laminar structure of g-C_3N_4 nanosheets would help the composite membranes to absorb the water molecules, which also promotes the construction of hydrophilic channels.[20] The increment of both the ADL and WU is also originated from the hydrophilic nature of g-C_3N_4. Although PBI/g-C_3N_4_1.5 and PBI/g-C_3N_4_2.0

membranes contain more g-C_3N_4 fillers, the ADL and WU values of them decreased. It seems that the agglomerated regions observed by SEM hindered the efficient absorption of sulfuric acid and water as observed in other reported nanocomposite membranes.[34, 35] The larger water uptake results in the larger volume swelling of polymer membranes[36] so the volume change behavior of PBI/g-C_3N_4 composite membranes is similar to the water uptake behavior.

Table 1. Physicochemical properties of PBI, PBI/g-C_3N_4 composite membranes and Nafion 115

	ADL	WU (%)	ΔV (%)	σ ($mScm^{-1}$)
PBI	1.49 (±0.04)	21.7 (±1.5)	13.8 (±0.7)	24.7(±2.9)
PBI/g-C_3N_4_0.5	1.50 (±0.05)	24.4 (±0.2)	22.4 (±1.1)	31.0(±2.3)
PBI/g-C_3N_4_0.75	1.66 (±0.02)	26.5 (±0.1)	29.9 (±0.2)	35.4(±1.6)
PBI/g-C_3N_4_1.0	1.76 (±0.02)	27.5 (±0.1)	35.5 (±0.3)	38.8(±2.3)
PBI/g-C_3N_4_1.5	1.58 (±0.08)	26.3 (±0.3)	29.2 (±1.6)	34.4(±3.4)
PBI/g-C_3N_4_2.0	1.43 (±0.13)	24.1 (±2.6)	23.0 (±2.1)	32.6(±2.7)
Nafion 115	-	-	-	70.6(±0.3)

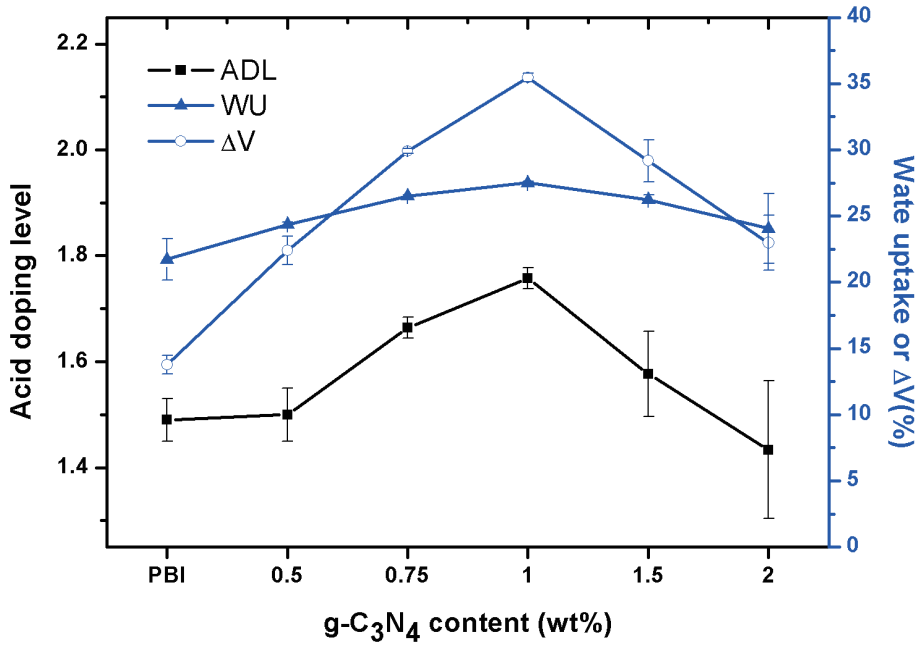

Figure 7. Acid doping level (ADL), water uptake (WU) and dimensional change (ΔV) of PBI and PBI/g-C_3N_4 composite membranes.

3.4. Proton conductivity and vanadium permeability

As the PBI/g-C_3N_4 composite membranes had improved ADL and WU values, which was discussed earlier, it was expected they would have higher proton conductivity in comparison to the PBI pristine membrane. The proton conductivity calculated from the area resistance of PBI, PBI/g-C_3N_4 composite membranes and Nafion 115 was shown in Table 1 and Figure 8. As expected, the proton conductivity of PBI/g-C_3N_4_1.0 membrane (38.8mScm^{-1}) was the highest among the composite membranes and the PBI pristine membrane (24.7mScm^{-1}). This is because the PBI/g-C_3N_4_1.0 membrane absorbed the largest amount of acid and water molecules which act as carriers in the vehicular mechanism or as hydrogen donors and acceptors forming hydrogen bond network in the Grotthus mechanism.[37, 38] However, when the g-C_3N_4 nanosheets content exceeded 1.0wt%, the proton conductivity began to decrease, which might be ascribed to the blocking of the proton pathway resulting from the agglomerated g-C_3N_4 nanofillers.[39-41] Thus, it is found that the optimum content of the g-C_3N_4 in order

to build an effective proton transport pathway is 1.0wt%.

Vanadium ion permeability is a crucial factor to evaluate a membrane as a separator of VRFB, since the high permeability for vanadium ions can cause low CEs and a rapid self-discharge rate. The change of VO^{2+} concentration diffused across the membrane was monitored with regular time intervals. (Fig. 9a) The PBI/g-C_3N_4_1.0 membrane having the highest proton conductivity was compared with PBI pristine and Nafion 115 membrane in terms of the vanadium permeability. Apparently, Nafion 115 showed the highest VO^{2+} diffusion rate owing to its large ion cluster channels.[42] On the other hand, PBI and PBI/g-C_3N_4 composite membrane exhibited extremely lower vanadium permeation with following reasons; the positively charged basic heterocyclic groups in the acid-doped PBI and g-C_3N_4 would repulse the vanadium cations (Donnan exclusion) and there is no microphase separation in PBI, unlike Nafion 115.[43, 44]

The permeability (P) values for VO^{2+} of Nafion 115, PBI and PBI/g-C_3N_4_1.0 membranes were calculated to $8.79 \times 10^{-7}, 7.86 \times 10^{-9}$ and 10.7×10^{-9} cm^2min^{-1}, respectively. The permeability of the PBI and PBI/g-C_3N_4_1.0

membranes was two orders of magnitude lower than that of Nafion 115 membrane. The vanadium permeability after the introduction of g-C_3N_4 nanosheets was slightly increased as a result of the greater acid and water absorption with enlarged ion transport channel.

In order to evaluate the combination effect of the proton conductivity and vanadium permeability of a membrane, the selectivity was compared in Fig. 9b. Despite the high proton conductivity, the selectivity of Nafion 115 (8.0×10^4S min cm^{-1}) was remarkably low, which was dominated by the significantly high vanadium permeability. In addition, the selectivity of PBI/g-C_3N_4_1.0 (3.1×10^6S min cm^{-1}) was higher than that of the PBI pristine membrane (3.6×10^6S min cm^{-1}), indicating the increase in proton conductivity of PBI/g-C_3N_4_1.0 more than compensated for the increase in vanadium permeability.

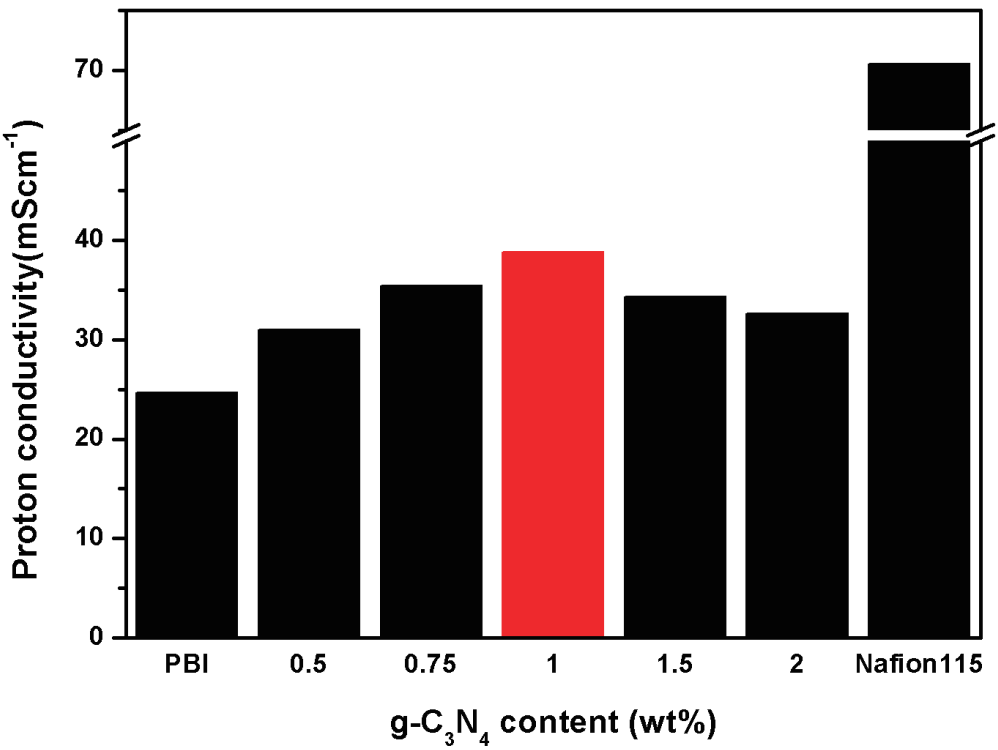

Figure 8. Proton conductivity of PBI, PBI/g-C_3N_4 composite membranes and Nafion115.

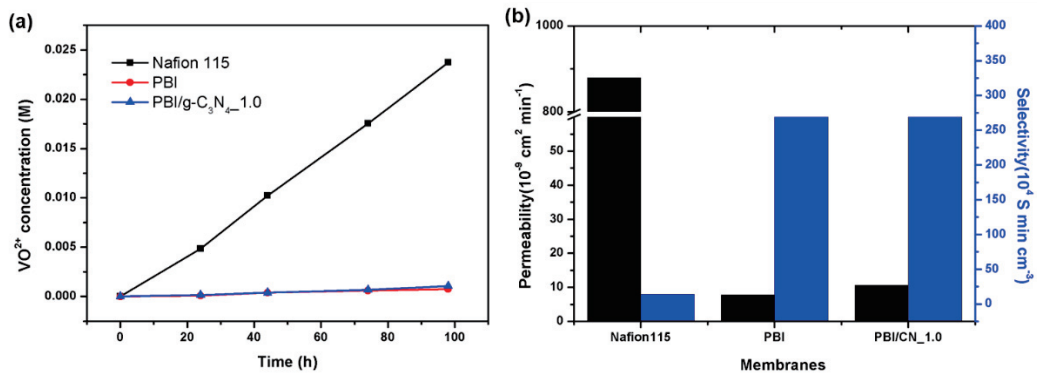

Figure 9. Concentration change of VO^{2+} over diffusion time (a), vanadium permeability and ion selectivity (b) of PBI, PBI/g-C_3N_4_1.0 and Nafion115.

3.5. VRFB single cell performance

VRFB single cell tests were performed with PBI and PBI/g-C_3N_4_1.0 membranes under current densities of 40-100mAcm^{-1} since PBI/g-C_3N_4_1.0 had the highest selectivity. The relationship between efficiency (CE, VE, and EE) and current density was illustrated in Fig. 10. CE (Fig. 10a) is affected adversely by permeation of VO^{2+} ions so the CE of PBI/g-C_3N_4_1.0 increased with a current density because of shorter charge-discharge time.[45] While the PBI pristine membrane showed very high CEs (>99%), the PBI/g-C_3N_4_1.0 showed lower CEs (>97%) owing to the increased vanadium permeability. However, the VEs of the PBI/g-C_3N_4_1.0 (88-70%) was higher than that of the PBI (83-65%) under all current densities. Generally, VE is affected by the ohmic overpotential[46] so the lowered area resistance and increased proton conductivity of PBI/g-C_3N_4_1.0 membranes resulted in this improved VE. EE, which is a product of CE and VE, is the most important parameter representing the energy utilization in VRFB.[45] At 40mAcm-1, the EEs of PBI (84%) and PBI/g-C_3N_4_1.0 (85%) were similar

because there is large influence of vanadium permeability in the low current density. However, the single cell with the PBI/g-C_3N_4_1.0 (81-70%) exhibited distinctly better EEs compared with the cell with the PBI pristine membrane (77-66%) under 60, 80, and 100mAcm^{-1}. From this, again, we could conclude that the improvement of proton conductivity of the PBI/g-C_3N_4_1.0 composite membrane was larger than the loss of vanadium blocking ability, which was also proved by high selectivity value.

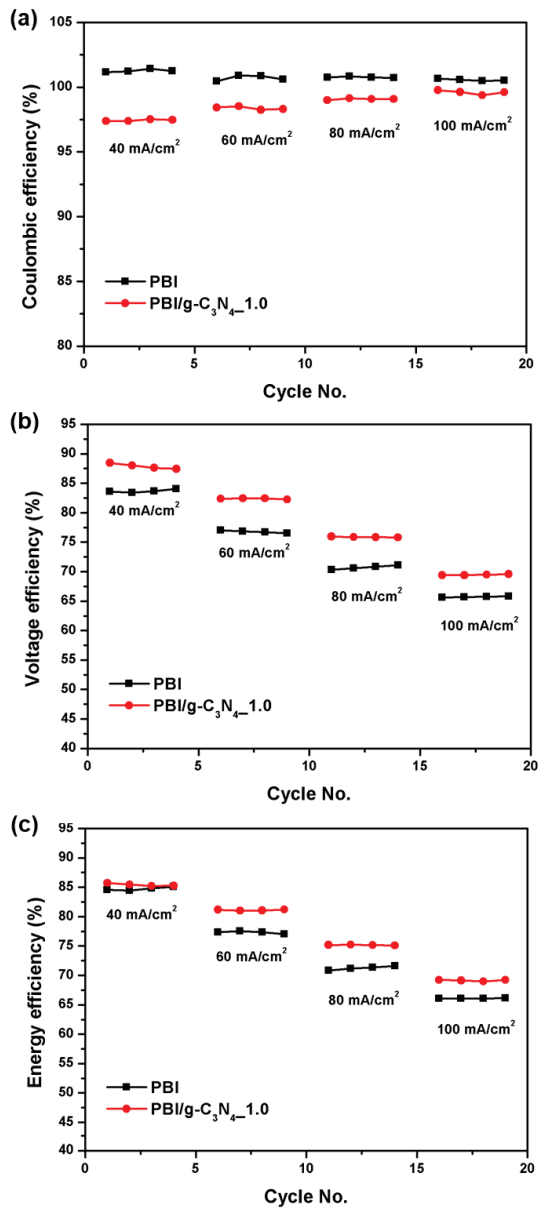

Figure 9. The VRFB single cell performance with PBI and PBI/g-C_3N_4_1.0 membranes under different current densities. (a) CE, (b) VE and (c) EE.

3.5. *Ex situ* oxidative stability

The *ex situ* chemical stability of the Nafion 115, PBI and PBI/g-C_3N_4 composite membranes was carried out in 0.1M VO_2^+ in 3M H_2SO_4 solutions at 40℃ for 700h (Fig. 11) The oxidation state of a sample membrane can be determined by observing the concentration change of V^{4+} ions produced from the reduction of V^{5+} ions. PBIs are known for their high chemical stability, which is ascribed to the electron deficient aromatic groups in their structure.[46, 47] The reference values were used for the VO^{2+} concentration change of the solution containing SPEEK, which was tested under the similar oxidative condition.[48] Nafion 115 had the best oxidative stability as expected and it was found that the relatively rapid degradation occurred in the SPEEK membrane. The VO^{2+} concentration of the solutions containing PBI/g-C_3N_4 composite membranes remained low, which is comparable to that of the solution containing the PBI membrane. From this result, it is demonstrated that the composite membranes of PBI with g-C_3N_4 nanosheets maintained the excellent oxidative stability of the

pristine PBI and thus, in turn, it is expected that they can be applied to the long-term VRFB operation.[49]

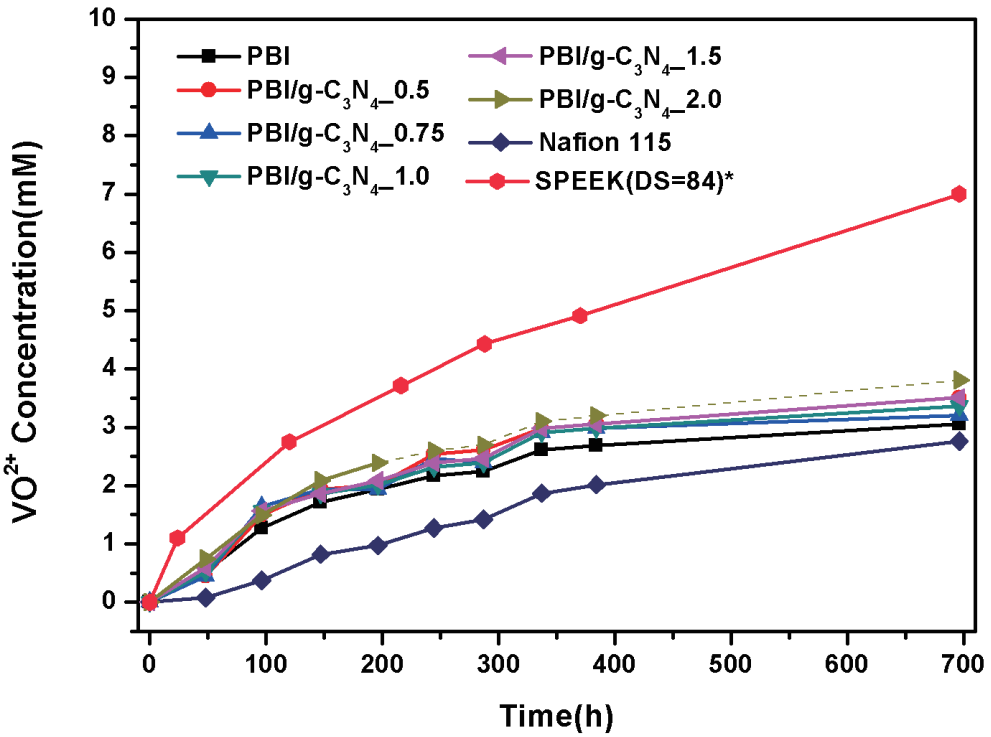

* reference data [48]

Figure 11. *Ex situ* chemical stability of PBI, PBI/g-C_3N_4 composite membranes and Nafion115.

4. Conclusion

Polybenzimidazole (PBI) composite membranes were prepared using graphitic carbon nitride (g-C3N4) nanosheets for the first time. The acid doping level and the water uptake of PBI/g-C_3N_4 composite membranes increased because of hydrophilic nature and the structural properties of g-C_3N_4 nanofillers. All PBI/g-C_3N_4 composite membranes exhibited better proton conductivity in comparison to pristine PBI. Given that the PBI/g-C3N4_1.0 membrane had the highest proton conductivity, the optimum filler content was found to be 1.0wt%. Although the PBI/g-C_3N_4_1.0 membrane showed slightly increased vanadium permeability compared to the pristine PBI, the vanadium permeability of PBI/g-C_3N_4_1.0 was still much lower than that of Nafion 115. Therefore, the VRFB single cell with PBI/g-C_3N_4_1.0 exhibited higher energy efficiency than the cell with PBI. PBI/g-C_3N_4 composite membranes maintained the good chemical stability of PBI. Therefore, we believe that the incorporation of g-C_3N_4 as a filler with PBI can be a promising strategy to develop ion exchange membranes for VRFB applications.

5. References

1. Bülbül, E.; Atanasov, V.; Mehlhorn, M.; Bürger, M.; Chromik, A.; Häring, T.; Kerres, J., Highly phosphonated polypentafluorostyrene blended with polybenzimidazole: Application in vanadium redox flow battery. *Journal of Membrane Science* **2019,** *570-571*, 194-203.

2. Peng, S.; Wu, X.; Yan, X.; Gao, L.; Zhu, Y.; Zhang, D.; Li, J.; Wang, Q.; He, G., Polybenzimidazole membranes with nanophase-separated structure induced by non-ionic hydrophilic side chains for vanadium flow batteries. *Journal of Materials Chemistry A* **2018,** *6* (9), 3895-3905.

3. Dunn, B.; Kamath, H.; Tarascon, J. M., Electrical energy storage for the grid: a battery of choices. *Science* **2011,** *334* (6058), 928-35.

4. Yang, Z.; Zhang, J.; Kintner-Meyer, M. C.; Lu, X.; Choi, D.; Lemmon, J. P.; Liu, J., Electrochemical energy storage for green grid. *Chem Rev* **2011,** *111* (5), 3577-613.

5. Ulaganathan, M.; Aravindan, V.; Yan, Q.; Madhavi, S.; Skyllas-Kazacos, M.; Lim, T. M., Recent Advancements in All-Vanadium Redox Flow Batteries. *Advanced Materials Interfaces* **2016,** *3* (1).

6. Parasuraman, A.; Lim, T. M.; Menictas, C.; Skyllas-Kazacos, M., Review of material research and development for vanadium redox flow battery applications. *Electrochimica Acta* **2013,** *101*, 27-40.

7. Li, X.; Zhang, H.; Mai, Z.; Zhang, H.; Vankelecom, I., Ion exchange membranes for vanadium redox flow battery (VRB) applications. *Energy & Environmental Science* **2011,** *4* (4).

8. Takimoto, N.; Wu, L.; Ohira, A.; Takeoka, Y.; Rikukawa, M., Hydration behavior of perfluorinated and hydrocarbon-type proton exchange membranes: Relationship between morphology and proton conduction. *Polymer* **2009,** *50* (2), 534-540.

9. Xi, J.; Wu, Z.; Qiu, X.; Chen, L., Nafion/SiO2 hybrid membrane for vanadium redox flow battery. *Journal of Power Sources* **2007,** *166* (2), 531-536.
10. Zhou, X. L.; Zhao, T. S.; An, L.; Wei, L.; Zhang, C., The use of polybenzimidazole membranes in vanadium redox flow batteries leading to increased coulombic efficiency and cycling performance. *Electrochimica Acta* **2015,** *153*, 492-498.
11. Wang, J. T.; Savinell, R. F.; Wainright, J.; Litt, M.; Yu, H., A fuel cell using acid doped polybenzimidazole as polymer electrolyte. *Electrochimica Acta* **1996,** *41* (2), 193-197.
12. Hu, M.; Ni, J.; Zhang, B.; Neelakandan, S.; Wang, L., Crosslinked polybenzimidazoles containing branching structure as membrane materials with excellent cell performance and durability for fuel cell applications. *Journal of Power Sources* **2018,** *389*, 222-229.
13. Xia, Z.; Ying, L.; Fang, J.; Du, Y.-Y.; Zhang, W.-M.; Guo, X.; Yin, J., Preparation of covalently cross-linked sulfonated polybenzimidazole membranes for vanadium redox flow battery applications. *Journal of Membrane Science* **2017,** *525*, 229-239.
14. Tian, X.; Wang, S.; Li, J.; Liu, F.; Wang, X.; Chen, H.; Wang, D.; Ni, H.; Wang, Z., Benzimidazole grafted polybenzimidazole cross-linked membranes with excellent PA stability for high-temperature proton exchange membrane applications. *Applied Surface Science* **2019,** *465*, 332-339.
15. Ding, L.; Song, X.; Wang, L.; Zhao, Z., Enhancing proton conductivity of polybenzimidazole membranes by introducing sulfonate for vanadium redox flow batteries applications. *Journal of Membrane Science* **2019,** *578*, 126-135.
16. Song, X.; Ding, L.; Wang, L.; He, M.; Han, X., Polybenzimidazole membranes embedded with ionic liquids for use in high proton selectivity vanadium redox flow batteries. *Electrochimica Acta* **2019,** *295*, 1034-1043.
17. Cai, Y.; Yue, Z.; Xu, S., A novel polybenzimidazole composite modified by sulfonated graphene oxide for high temperature proton exchange membrane fuel cells in anhydrous atmosphere. *Journal of Applied Polymer Science* **2017,** *134* (25).
18. Shi, Y.; Jiang, S.; Zhou, K.; Bao, C.; Yu, B.; Qian, X.; Wang, B.; Hong, N.; Wen, P.; Gui, Z.; Hu, Y.; Yuen, R. K., Influence of g-C3N4 nanosheets on thermal stability and mechanical properties of biopolymer electrolyte nanocomposite films: a

novel investigation. *ACS Appl Mater Interfaces* **2014,** *6* (1), 429-37.

19. Niu, P.; Zhang, L.; Liu, G.; Cheng, H.-M., Graphene-Like Carbon Nitride Nanosheets for Improved Photocatalytic Activities. *Advanced Functional Materials* **2012,** *22* (22), 4763-4770.

20. Niu, R.; Kong, L.; Zheng, L.; Wang, H.; Shi, H., Novel graphitic carbon nitride nanosheets/sulfonated poly(ether ether ketone) acid-base hybrid membrane for vanadium redox flow battery. *Journal of Membrane Science* **2017,** *525*, 220-228.

21. Wang, L.; Yu, L.; Mu, D.; Yu, L.; Wang, L.; Xi, J., Acid-base membranes of imidazole-based sulfonated polyimides for vanadium flow batteries. *Journal of Membrane Science* **2018,** *552*, 167-176.

22. Kim, T.-H.; Lim, T.-W.; Lee, J.-C., High-temperature fuel cell membranes based on mechanically stable para-ordered polybenzimidazole prepared by direct casting. *Journal of Power Sources* **2007,** *172* (1), 172-179.

23. Lotsch, B. V.; Doblinger, M.; Sehnert, J.; Seyfarth, L.; Senker, J.; Oeckler, O.; Schnick, W., Unmasking melon by a complementary approach employing electron diffraction, solid-state NMR spectroscopy, and theoretical calculations-structural characterization of a carbon nitride polymer. *Chemistry* **2007,** *13* (17), 4969-80.

24. Thomas, A.; Fischer, A.; Goettmann, F.; Antonietti, M.; Müller, J.-O.; Schlögl, R.; Carlsson, J. M., Graphitic carbon nitride materials: variation of structure and morphology and their use as metal-free catalysts. *Journal of Materials Chemistry* **2008,** *18* (41).

25. Raymundo-Piñero, E.; Cazorla-Amorós, D.; Linares-Solano, A.; Find, J.; Wild, U.; Schlögl, R., Structural characterization of N-containing activated carbon fibers prepared from a low softening point petroleum pitch and a melamine resin. *Carbon* **2002,** *40* (4), 597-608.

26. Wang, X.; Maeda, K.; Thomas, A.; Takanabe, K.; Xin, G.; Carlsson, J. M.; Domen, K.; Antonietti, M., A metal-free polymeric photocatalyst for hydrogen production from water under visible light. *Nat Mater* **2009,** *8* (1), 76-80.

27. Yang, S.; Gong, Y.; Zhang, J.; Zhan, L.; Ma, L.; Fang, Z.; Vajtai, R.; Wang, X.; Ajayan, P. M., Exfoliated graphitic carbon nitride nanosheets as efficient catalysts for hydrogen evolution under visible light. *Adv Mater* **2013,** *25* (17), 2452-6.

28. Jayabharathi, J.; Sundharesan, M.; Prabhakaran, A.; Karunakaran, C.,

Understanding the binding interaction of imidazole with ZnO nanomaterials and clusters. *RSC Advances* **2015,** *5* (13), 9518-9531.

29. Cao, K.; Jiang, Z.; Zhang, X.; Zhang, Y.; Zhao, J.; Xing, R.; Yang, S.; Gao, C.; Pan, F., Highly water-selective hybrid membrane by incorporating g-C3N4 nanosheets into polymer matrix. *Journal of Membrane Science* **2015,** *490*, 72-83.

30. Li, M.-Q.; Shao, Z.-G.; Scott, K., A high conductivity Cs2.5H0.5PMo12O40/polybenzimidazole (PBI)/H3PO4 composite membrane for proton-exchange membrane fuel cells operating at high temperature. *Journal of Power Sources* **2008,** *183* (1), 69-75.

31. Kyaw Zay, Y. A.; Kumazawa, K.; Kawamura, G.; Muto, H.; Matsuda, A., Cell performance enhancement with titania-doped polybenzimidazole based composite membrane in intermediate temperature fuel cell under anhydrous condition. *Journal of the Ceramic Society of Japan* **2018,** *126* (10), 789-793.

32. Khabashesku, V. N.; Zimmerman, J. L.; Margrave, J. L., Powder Synthesis and Characterization of Amorphous Carbon Nitride. *Chemistry of Materials* **2000,** *12* (11), 3264-3270.

33. Wainright, J. S., Acid-Doped Polybenzimidazoles: A New Polymer Electrolyte. *Journal of The Electrochemical Society* **1995,** *142* (7).

34. Lu, Y.; Pan, X.; Li, N.; Hu, Z.; Chen, S., Improved performance of quaternized poly(arylene ether ketone)s/graphitic carbon nitride nanosheets composite anion exchange membrane for fuel cell applications. *Applied Surface Science* **2020,** *503*.

35. Lee, H.; Han, J.; Kim, K.; Kim, J.; Kim, E.; Shin, H.; Lee, J.-C., Highly sulfonated polymer-grafted graphene oxide composite membranes for proton exchange membrane fuel cells. *Journal of Industrial and Engineering Chemistry* **2019,** *74*, 223-232.

36. Li, Q., Water uptake and acid doping of polybenzimidazoles as electrolyte membranes for fuel cells. *Solid State Ionics* **2004,** *168* (1-2), 177-185.

37. Liu, B.; Zhang, Y.; Jiang, Y.; Qian, P.; Shi, H., High performance acid-base composite membranes from sulfonated polysulfone containing graphitic carbon nitride nanosheets for vanadium redox flow battery. *Journal of Membrane Science* **2019,** *591*.

38. Peckham, T. J.; Holdcroft, S., Structure-morphology-property relationships of non-perfluorinated proton-conducting membranes. *Adv Mater* **2010,** *22* (42), 4667-90.

39. Chien, H.-C.; Tsai, L.-D.; Huang, C.-P.; Kang, C.-y.; Lin, J.-N.; Chang, F.-C.,

Sulfonated graphene oxide/Nafion composite membranes for high-performance direct methanol fuel cells. *International Journal of Hydrogen Energy* **2013,** *38* (31), 13792-13801.

40. Ko, T.; Kim, K.; Lim, M.-Y.; Nam, S. Y.; Kim, T.-H.; Kim, S.-K.; Lee, J.-C., Sulfonated poly(arylene ether sulfone) composite membranes having poly(2,5-benzimidazole)-grafted graphene oxide for fuel cell applications. *Journal of Materials Chemistry A* **2015,** *3* (41), 20595-20606.

41. Ahmad, A. L.; Farooqui, U. R.; Hamid, N. A., Effect of graphene oxide (GO) on Poly(vinylidene fluoride-hexafluoropropylene) (PVDF- HFP) polymer electrolyte membrane. *Polymer* **2018,** *142*, 330-336.

42. Jeong, S.; Kim, L.-H.; Kwon, Y.; Kim, S., Effect of nafion membrane thickness on performance of vanadium redox flow battery. *Korean Journal of Chemical Engineering* **2014,** *31* (11), 2081-2087.

43. Ding, L.; Song, X.; Wang, L.; Zhao, Z.; He, G., Preparation of dense polybenzimidazole proton exchange membranes with different basicity and flexibility for vanadium redox flow battery applications. *Electrochimica Acta* **2018,** *292*, 10-19.

44. Yuan, Z.; Duan, Y.; Zhang, H.; Li, X.; Zhang, H.; Vankelecom, I., Advanced porous membranes with ultra-high selectivity and stability for vanadium flow batteries. *Energy & Environmental Science* **2016,** *9* (2), 441-447.

45. Shi, Y.; Eze, C.; Xiong, B.; He, W.; Zhang, H.; Lim, T. M.; Ukil, A.; Zhao, J., Recent development of membrane for vanadium redox flow battery applications: A review. *Applied Energy* **2019,** *238*, 202-224.

46. Yang, D.-S.; Lee, J. Y.; Jo, S.-W.; Yoon, S. J.; Kim, T.-H.; Hong, Y. T., Electrocatalytic activity of nitrogen-doped CNT graphite felt hybrid for all-vanadium redox flow batteries. *International Journal of Hydrogen Energy* **2018,** *43* (3), 1516-1522.

47. Li, Q.; He, R.; Jensen, J. O.; Bjerrum, N. J., PBI-Based Polymer Membranes for High Temperature Fuel Cells– Preparation, Characterization and Fuel Cell Demonstration. *Fuel Cells* **2004,** *4* (3), 147-159.

48. Yuan, Z.; Li, X.; Hu, J.; Xu, W.; Cao, J.; Zhang, H., Degradation mechanism of sulfonated poly(ether ether ketone) (SPEEK) ion exchange membranes under vanadium flow battery medium. *Phys Chem Chem Phys* **2014,** *16* (37), 19841-7.

49. Chen, D.; Qi, H.; Sun, T.; Yan, C.; He, Y.; Kang, C.; Yuan, Z.; Li, X.,

Polybenzimidazole membrane with dual proton transport channels for vanadium flow battery applications. *Journal of Membrane Science* **2019,** *586*, 202-210.

국문 요약

폴리벤지미다졸(PBI)은 바나듐 레독스 흐름 전지(VRFB)의 이온 교환막으로서 매우 높은 바나듐 이온 투과도 및 높은 화학적 안정성으로 인해 널리 사용되어왔다. 그러나 PBI의 비교적 낮은 수소 이온 전도도는 상업화된 나피온과 비교하여 낮은 전지 성능을 야기한다. 따라서, 열 산화 및 박리 과정을 통해 얻은 그래피틱 카본 나이트라이드 ($g-C_3N_4$) 나노시트를 첨가제로 하여 PBI/$g-C_3N_4$ 복합막을 제조하였다. $g-C_3N_4$의 구조적 특징은 추가적인 산 도핑 사이트를 제공하고 안전한 수소 이온 전도 채널 형성을 만드는 것을 돕는다. PBI/$g-C_3N_4$ 복합막은 PBI 막과 비교하여 높은 황산 도핑 레벨과 함수량을 나타냈으며 따라서 수소 이온 전도도가 향상되었다. 그리고 $g-C_3N_4$가 1.0 무게 비율만큼 포함된 PBI/$g-C_3N_4$_1.0 막이 가장 높은 수소 이온 전도도를 가졌다. PBI와 PBI/$g-C_3N_4$_1.0 복합막은 모두 나피온보다 현저히 낮은 바나듐 투과도를 가졌다. VRFB 싱글 셀 테스트 결과에서, PBI/$g-C_3N_4$_1.0 복합막을 이용한 셀의 에너지 효율이 PBI막을 이용했을 때보다 향상되었다. 또한, $g-C_3N_4$를 도입하여도 PBI의

좋은 산화안정성을 저하시키지 않는 것을 확인하였다.

주요어: 폴리벤지미다졸, 그래피틱 카본 나이트라이드, 복합막, 이온교환막, 바나듐 레독스 흐름 전지

학번: 2018-22675